Exceedingly small iron oxide nanoparticles as positive MRI contrast agents

He Wei[a,1], Oliver T. Bruns[a,1], Michael G. Kaul[b,1], Eric C. Hansen[a], Mariya Barch[c], Agata Wiśniowska[d], Ou Chen[e], Yue Chen[a], Nan Li[c,f,g], Satoshi Okada[c], Jose M. Cordero[a], Markus Heine[h], Christian T. Farrar[i], Daniel M. Montana[a,j], Gerhard Adam[b], Harald Ittrich[b], Alan Jasanoff[c,f,g], Peter Nielsen[h], and Moungi G. Bawendi[a,2]

[a]Department of Chemistry, Massachusetts Institute of Technology, Cambridge, MA 02139; [b]Department of Diagnostic and Interventional Radiology and Nuclear Medicine, Center for Radiology and Endoscopy, University Medical Center Hamburg-Eppendorf, 20246 Hamburg, Germany; [c]Department of Biological Engineering, Massachusetts Institute of Technology, Cambridge, MA 02139; [d]Health Sciences and Technology, Massachusetts Institute of Technology, Cambridge, MA 02139; [e]Department of Chemistry, Brown University, Providence, RI 02912; [f]Department of Brain and Cognitive Sciences, Massachusetts Institute of Technology, Cambridge, MA 02139; [g]Department of Nuclear Science and Engineering, Massachusetts Institute of Technology, Cambridge, MA 02139; [h]Department of Biochemistry and Molecular Cell Biology, University Medical Center Hamburg-Eppendorf, 20246 Hamburg, Germany; [i]Athinoula A. Martinos Center for Biomedical Imaging, Massachusetts General Hospital and Harvard Medical School, Charlestown, MA 02129; and [j]Department of Materials Science and Engineering, Massachusetts Institute of Technology, Cambridge, MA 02139

Contributed by Moungi G. Bawendi, December 23, 2016 (sent for review November 2, 2016; reviewed by Kevin Bennett and Jin Xie)

Medical imaging is routine in the diagnosis and staging of a wide range of medical conditions. In particular, magnetic resonance imaging (MRI) is critical for visualizing soft tissue and organs, with over 60 million MRI procedures performed each year worldwide. About one-third of these procedures are contrast-enhanced MRI, and gadolinium-based contrast agents (GBCAs) are the mainstream MRI contrast agents used in the clinic. GBCAs have shown efficacy and are safe to use with most patients; however, some GBCAs have a small risk of adverse effects, including nephrogenic systemic fibrosis (NSF), the untreatable condition recently linked to gadolinium (Gd) exposure during MRI with contrast. In addition, Gd deposition in the human brain has been reported following contrast, and this is now under investigation by the US Food and Drug Administration (FDA). To address a perceived need for a Gd-free contrast agent with pharmacokinetic and imaging properties comparable to GBCAs, we have designed and developed zwitterion-coated exceedingly small superparamagnetic iron oxide nanoparticles (ZES-SPIONs) consisting of ∼3-nm inorganic cores and ∼1-nm ultrathin hydrophilic shell. These ZES-SPIONs are free of Gd and show a high T_1 contrast power. We demonstrate the potential of ZES-SPIONs in preclinical MRI and magnetic resonance angiography.

exceedingly small iron oxide nanoparticles | renal clearance | gadolinium-free positive MR contrast agent | preclinical magnetic resonance imaging

MRI signal arises from the excitation of low-energy nuclear spins, which are formed in a permanent magnetic field, by applying radiofrequency pulses followed by the measurement of the spin relaxation processes (i.e., T_1 recovery or T_2 decay) (1, 2). Different chemical environments as well as water concentration result in different signal strengths and therefore provide contrast between fat, tissue, and bones. Paramagnetic compounds can be used to enhance the contrast of MR images by promoting relaxation of water near the compound. MRI contrast agents are classified as either T_1 (i.e., positive) or T_2 (i.e., negative). Radiologists strongly prefer T_1 contrast agents because T_2 contrast shows as darkened areas, which can be difficult to distinguish from internal bleeding, air–tissue boundaries (3), or other susceptibility artifacts, resulting in less accurate patient diagnosis. We also note that progress has been made to generate positive contrast by artificially turning dark and susceptibility-related negative contrast bright (4). Moreover, T_1 relaxation times in animal tissues are generally much longer than their T_2 relaxation times, meaning that the relaxivity of the T_1 contrast agent can be smaller than that for a T_2 agent to obtain the same amount of change in image intensity. All gadolinium (Gd)-based contrast agents (GBCAs) (5–9) used in the clinic today are T_1 contrast agents (10), whereas GBCAs still have a small risk of adverse effects including nephrogenic systemic fibrosis (11, 12) and Gd deposition in the human brain (13–16).

Superparamagnetic iron oxide nanoparticles (SPIONs) are single-domain magnetic iron oxide particles with hydrodynamic diameters (HDs) ranging from single nanometers to >100 nm (17–19). SPIONs can be monodisperse and coated by biologically compatible ligands, are chemically and biologically stable, and are generally nontoxic in vivo (20). However, commercially available SPION contrast agents are composed of polydisperse inorganic cores with large HD, ranging from ∼16 to ∼200 nm. Generally, large SPIONs function as T_2 contrast agents, whereas small SPIONs have limited T_2 activity and therefore are potential T_1 contrast agents. In addition, due to their large HD, existing SPIONs (21) prevent efficient renal clearance after i.v. administration, greatly differing from GBCA elimination pathways. As a result, large HD SPIONs predominately accumulate in the body (22) and can cause a persistent negative contrast over several weeks or months, which prevents repeated imaging studies and limits the clinical management of patients. Furthermore, current SPION formulations are almost quantitatively metabolized and absorbed into the iron pool with the potential of

Significance

Gadolinium (Gd)-based contrast agents (GBCAs) are currently the mainstream clinical MRI contrast agents. Some GBCAs have shown a long-term toxicity—nephrogenic systemic fibrosis (NSF)—and Gd depositions in the brain. The NSF has triggered a Food and Drug Administration (FDA) black-box warning and a contraindication of some GBCAs. The finding of Gd depositions led to an ongoing FDA investigation to monitor their possible long-term adverse effects. Here, we present T_1-weighted contrast-enhanced MR imaging and angiography using zwitterion-coated exceedingly small superparamagnetic iron oxide nanoparticles (ZES-SPIONs) in mice and rats. Renal clearance and biodistribution results further demonstrate that ZES-SPIONs are qualitatively different from previously reported SPIONs. This work may open up opportunities to develop exceedingly small SPIONs that show effective T_1 contrast as Gd-free alternatives to GBCAs.

Author contributions: H.W., O.T.B., and M.G.B. designed research; H.W., O.T.B., M.G.K., E.C.H., M.B., A.W., Y.C., M.H., C.T.F., and P.N. performed research; H.W. contributed new reagents/analytic tools; H.W., O.T.B., M.G.K., E.C.H., M.B., A.W., O.C., Y.C., N.L., S.O., J.M.C., C.T.F., D.M.M., H.I., and P.N. analyzed data; and H.W., O.T.B., M.G.K., G.A., A.J., and M.G.B. wrote the paper.

Reviewers: K.B., University of Hawaii at Manoa; and J.X., University of Georgia.

The authors declare no conflict of interest.

[1]H.W., O.T.B., and M.G.K. contributed equally to this work.

[2]To whom correspondence should be addressed. Email: mgb@mit.edu.

This article contains supporting information online at www.pnas.org/lookup/suppl/doi:10.1073/pnas.1620145114/-/DCSupplemental.

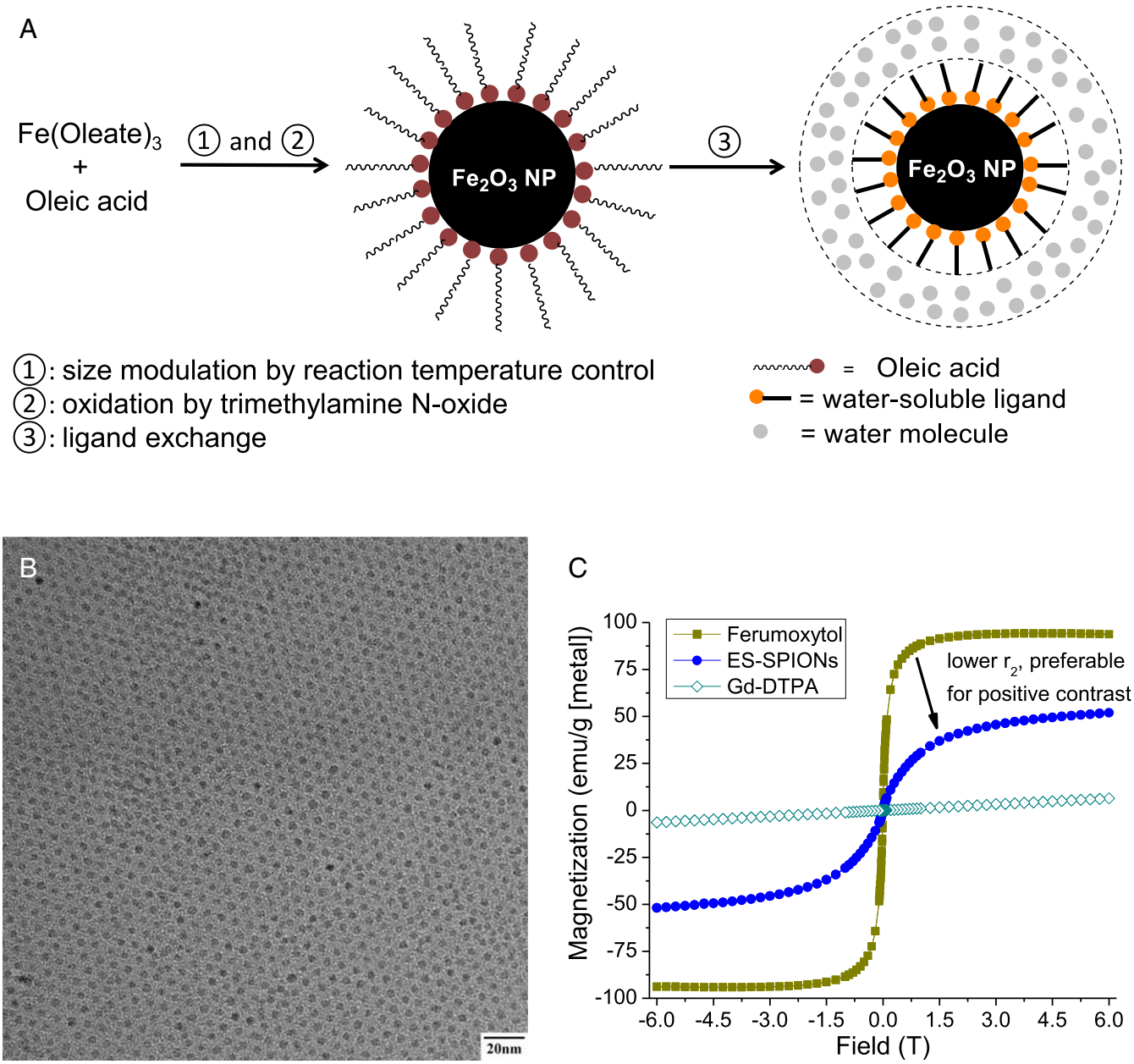

Fig. 1. (*A*) Rationally designed synthetic route of ZDS-coated SPIONs, (*B*) HR-TEM images of SPIONs with ~3.0-nm inorganic core diameter, and (*C*) SQUID curves of 3-nm ES-SPIONs, ferumoxytol (Feraheme), as well as Gd-DTPA (Magnevist).

clinical side effects from iron overload (22). We note that the development and production of existing SPION-based MRI contrast agents, including Resovist, Feridex, Combidex, Supravist, Clariscan (21), and Gastromark (23, 24), has largely ceased. Hence, there is a perceived need for developing Gd-free SPIONs that are exceedingly small for T_1-weighted MRI and as a potential substitute for GBCAs. In contrast to previous large HD SPIONs, and to address the perceived need for a Gd-free positive contrast agent, we have designed zwitterion-coated exceedingly small superparamagnetic iron oxide nanoparticles (ZES-SPIONs) with two considerations: (*i*) optimizing T_1 contrast and (*ii*) enabling renal clearance. Optimizing T_1 contrast (25) for SPIONs translates into minimizing the ratio r_2/r_1 while preserving an absolute r_1 value similar to GBCAs, where r_2 and r_1 are the transverse and longitudinal relaxivities, respectively (26). We achieve this by using the less magnetic maghemite (Fe_2O_3) structure, which shows a lower magnetization at clinical strength (1.5 T) applied magnetic fields (27, 28), as opposed to the magnetite (Fe_3O_4) structure (29), and this translates into a correspondingly low T_2 effect (30, 31). To enable renal clearance, ZES-SPIONs must have a HD below ~5.5 nm and show minimal nonspecific interactions (i.e., minimal biofouling) in vivo (32), which renders ZES-SPIONs as ideal candidates for future targeted imaging applications. Most existing SPIONs described for biomedical applications (21) have an HD greater than 7 nm. Hence, there is a perceived need for developing Gd-free SPIONs that are exceedingly small for T_1-weighted MRI and enhanced renal clearance as potential substitutes for GBCAs. Here, we show that ZES-SPIONs as T_1 contrast agents are indeed qualitatively different from existing SPIONs (21) and indeed approach the performance properties of GBCAs.

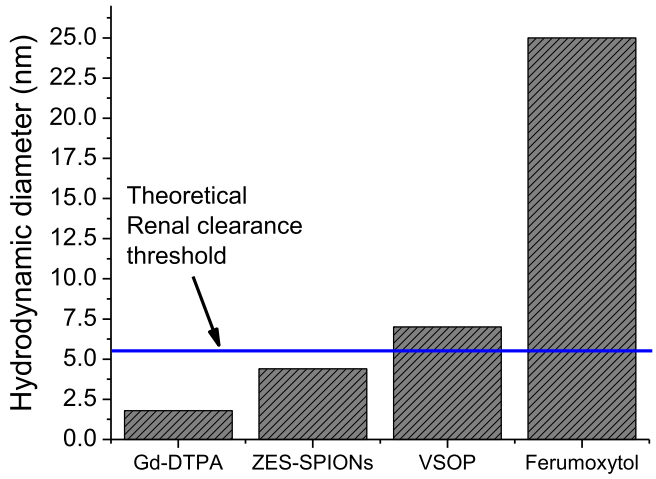

Field Strength (T)		Core (nm)	HD (nm)	r_1 ($s^{-1}mM^{-1}$)	r_2 ($s^{-1}mM^{-1}$)	r_2/r_1
1.5	Gd-DTPA	Gd^{3+}	1.8	4.8	5.1	1.1
	ZES-SPIONs	3	4.7	5.2	10.5	2.0
	VSOP	4	7	15	32	2.1
	Ferumoxytol	7	20-30	15	89	5.9
7	Gd-DTPA	Gd^{3+}	1.8	3.1	5.4	1.7
	ZES-SPIONs	3	4.4	1.5	17	11
	Ferumoxytol	7	20-30	3.1	68	22

Fig. 2. HD and T_1 contrast power of different contrast agents (ferumoxytol, Feraheme; Gd-DTPA, Magnevist; VSOP, very small iron oxide nanoparticles; ZES-SPIONs, zwitterion-coated exceedingly small iron oxide nanoparticles).

Our SPIONs were synthesized from the thermal decomposition of $Fe(oleate)_3$ in the presence of oleic acid and in solvent mixtures rationally designed for tuning their boiling point. This is followed by oxidation with trimethylamine N-oxide (Fig. 1*A*) (33). The oxidation step ensures particles with a maghemite structure. Syntheses of SPIONs with a range of ∼2.5- to ∼7.0-nm inorganic core diameters were produced with narrow size distribution by adjusting the solvent mixture boiling point, using mixtures of 1-tetradecene (TDE), 1-hexadecene (HDE), and 1-octadecene (ODE), keeping both the concentration of precursors and growth time constant (Fig. S1) (34, 35). Fig. 1*B* shows a high-resolution transmission electron microscopy (HR-TEM) image of ∼3.0-nm SPIONs. Relaxivity results at 7 T show that this size provides good T_1-weighted MRI signal (Table S1). We characterized the magnetic behavior of ∼3.0-nm SPIONs coated in native ligands at room temperature (298K) using a superconducting quantum interference device (SQUID) and compared it to the commercially available and US Food and Drug Administration (FDA)-approved ferumoxytol (Feraheme), which consists of 3- to 10-nm mixed magnetite/maghemite cores [confirmed by X-ray powder diffraction (XRD) in Fig. S2]. In Fig. 1*C*, the superparamagnetism of our ∼3-nm SPIONs at room temperature is confirmed by the absence of a hysteresis loops near zero field. Fig. 1*C* also shows that Gd-DTPA (Magnevist) has a small magnetization (M), desired for T_1-weighted MRI. In the range of clinical magnetic field strengths (1.5–3 T), Fig. 1*C* shows that the M of magnetite-containing ferumoxytol is 94 emu/g [Fe], whereas the M of our ∼3-nm SPIONs is only 35 emu/g [Fe]. Assuming the magnetic volume/field gradient and water-SPION interaction are largely unchanged, this low M would yield a reduced r_2 relaxivity and an enhanced T_1-weighted MRI signal, a strategy that has been successfully used for doped ferritin-based SPIONs (36).

After synthesizing the above inorganic core SPIONs, the native hydrophobic oleic acid coating was exchanged with a zwitterionic dopamine sulfonate (ZDS) that we have previously developed and described (35, 37). Our prior studies have demonstrated that ZDS-coated SPIONs show small HDs, low nonspecific interactions in vitro with cells and in vivo in mice, offering the opportunity for specific labeling, and stability with respect to time, pH, and salinity. Moreover, ZDS-coated SPIONs can retain the magnetic properties of as-synthesized hydrophobic SPIONs, making them useful for MRI. The biocompatibility of ZDS was also confirmed by other research groups on several types of nanoparticles (10, 38, 39). Fig. S3 shows the result of using HPLC with a size exclusion column to determine the HD of ∼3-nm core particles coated with ZDS (ZES-SPIONs), giving an average HD of 4.7 nm.

To quantitatively evaluate (40) the T_1 contrast power of ZES-SPIONs and differentiate it with previously reported agents, we compare the r_1 and r_2 values of ZES-SPIONs and other types of T_1 contrast agents (3, 30, 41). The data for ferumoxytol (42, 43), very-small iron oxide nanoparticles (VSOPs) (44), as well as Gd-DTPA (Magnevist) (24, 45) are either measured or taken from the published literature. As shown in Fig. 2, at 1.5 T, which is the field strength of most clinical MRI scanners, ZES-SPIONs with a 3-nm

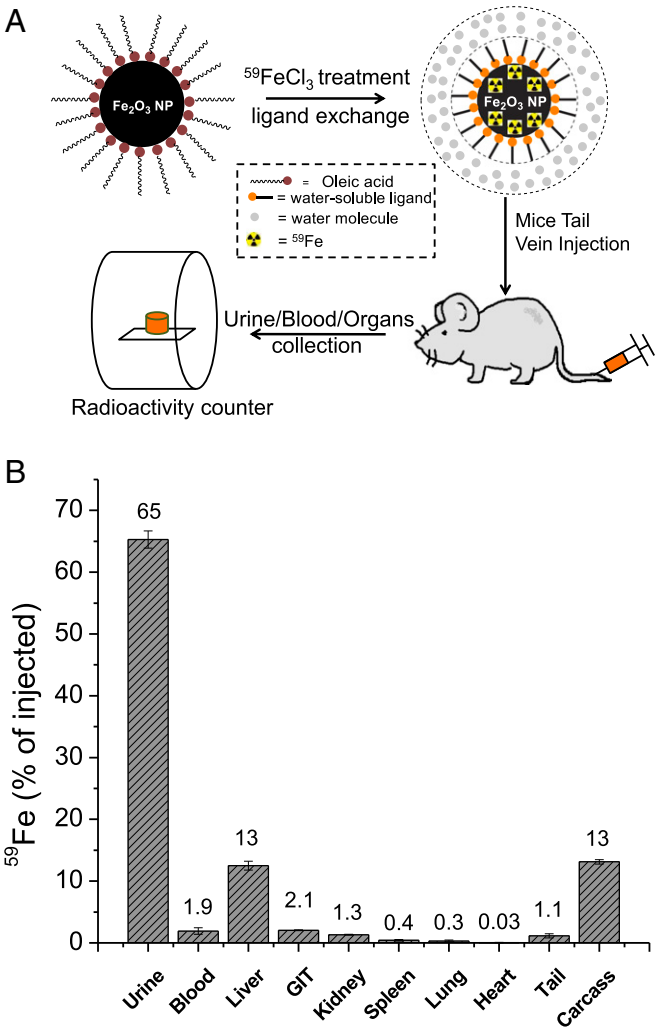

Fig. 3. (*A*) Schematic of mouse biodistribution study using ^{59}Fe-labeled ZES-SPIONs, and (*B*) the percentages of ^{59}Fe-labeled ZES-SPIONs that stay in urine, blood, and organs, compared with the total amount of ^{59}Fe-labeled ZES-SPIONs injected (GIT, gastrointestinal tract). After 24 h following injection, 12.5 ± 0.7% of the injected ^{59}Fe-labeled ZES-SPIONs remained in the liver. The combination of blood, spleen, kidney, lung, gastrointestinal tract, heart, carcass, and tail had less than 25% of the injected ^{59}Fe-labeled ZES-SPIONs.

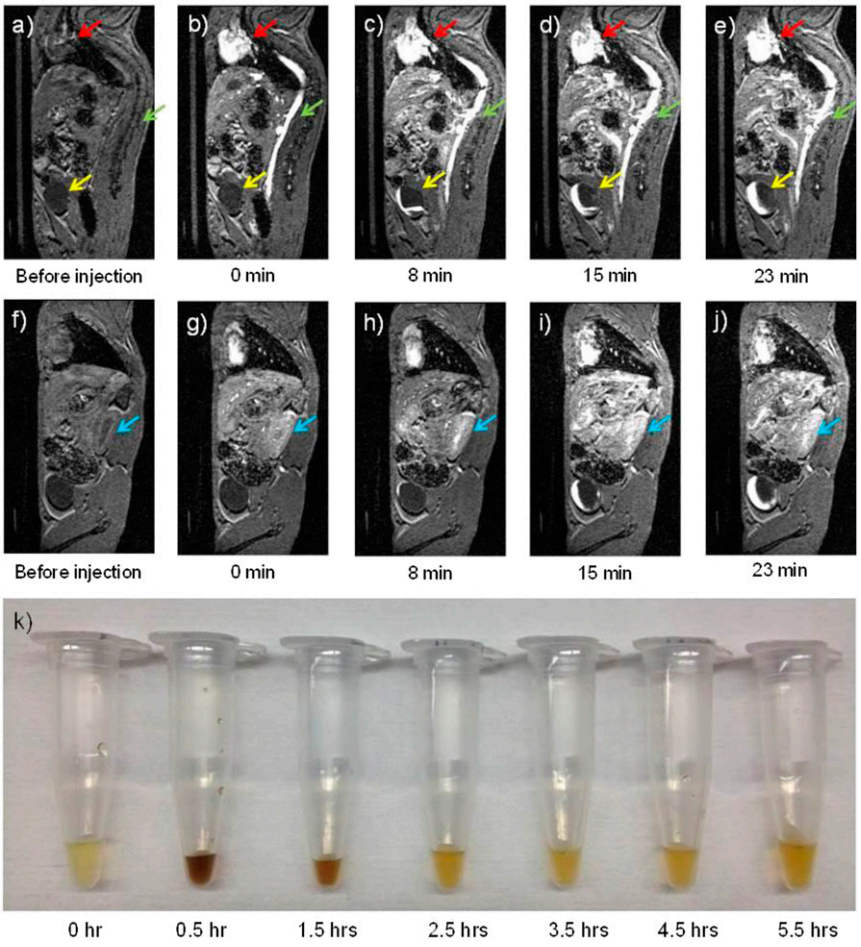

Fig. 4. (*A–J*) T_1-weighted MR images of a mouse injected with ZDS-coated exceedingly small SPIONs (ZES-SPIONs) at 7 T. Time points underneath each image: the time after ZES-SPIONs injection: (*A–E*) one sagittal slice showing the heart (red arrow), the vena cava (green arrow), and the bladder (yellow arrow), and (*F–J*) another sagittal slice showing the kidney (blue arrow); (*K*) urine samples from mice taken at different time points after injection showing renal clearance of ZES-SPIONs in vivo. Before the injection of ZES-SPIONs, the heart (red arrow), the vena cava (green arrow), and the bladder (yellow arrow) do not show appreciable positive contrast. After injection, the heart and the vena cava display high positive contrast immediately after injection. At 8 min after injection, the bladder displays some positive contrast, indicating an excretion of urine containing ZES-SPIONs. With the increase of time postinjection, Fig. 4 *D* and *E* shows that the positive contrast region of the bladder increases, suggesting an accumulation of urine with ZES-SPIONs.

inorganic core and a 4.7-nm HD have an r_1 of 5.2 $s^{-1}{\cdot}mM^{-1}$ and r_2 of 10.5 $s^{-1}{\cdot}mM^{-1}$, leading to an r_2/r_1 of 2.0, which is three times smaller than the r_2/r_1 of the commercially available SPION-based ferumoxytol. The r_2/r_1 of ZES-SPIONs is slightly lower and therefore slightly better than that of VSOP (44), a state-of-the-art SPION-based T_1 contrast agent. The r_2/r_1 of our ZES-SPIONs is more preferable than that of other SPION-based MRI contrast agents including Feraheme, Resovist, Feridex, Combidex, Supravist, Clariscan, and others (3, 8, 9, 21, 46, 47). Furthermore, as shown in Fig. 2, the r_2/r_1 of ZES-SPIONs at 1.5 T is within a factor of 2 to that of gadolinium-based chelates (GBCAs) such as Gd-DTPA. Crucially, not only do our ZES-SPIONs show a more promising r_2/r_1 than previous SPIONs, but they are also smaller and qualitatively different; unlike previous SPION-based T_1 contrast agents, the HD of ZES-SPIONs falls below the effective, expected renal clearance cutoff (i.e., the glomerular filtering threshold) of ∼5.5 nm as detailed below (32). The HD of ZES-SPIONs is 4.7 nm, which is approximately two times smaller than the HD of VSOP, and approximately six times smaller than the HD of ferumoxytol, respectively (Fig. 2).

To assess the in vivo stability of our ZES-SPION formulation, we designed and performed a biodistribution experiment using ^{59}Fe radioisotope-labeled ZES-SPIONs. As shown in Fig. 3*A*, ES-SPIONs were first labeled with ^{59}Fe (48) and then ligand exchanged with ZDS. The resulting radioactive ZES-SPIONs were analyzed by gel filtration chromatography (GFC) equipped with a size exclusion column, which showed the simultaneous elution of high radioactivity and ZES-SPIONs, indicating the successful incorporation of ^{59}Fe. The ^{59}Fe-labeled ZES-SPIONs were i.v. injected into mice. After 4 and 24 h, the urine and feces were collected and separated, and the ^{59}Fe concentration was measured by a radioactivity counter. As reported in Fig. 3*B*, 65 ± 1.4% of the injected ^{59}Fe-labeled ZES-SPIONs was renally cleared (most of it within 4 h). Organs and blood were collected 24 h postinjection, and the ^{59}Fe activity was measured to determine the biodistribution. Fig. 3*B* shows that, 24 h after injection, 13 ± 0.70% of the injected ^{59}Fe remained in the liver. However, the combination of blood, spleen, kidney, lung, gastrointestinal tract, heart, and tail had around 12%. The remaining carcass had around 13% of the injected ^{59}Fe. These results suggest that the majority of ZES-SPIONs are cleared through the renal route.

To further visualize renal clearance, our ZES-SPIONs were i.v. injected into mice and their urine was collected at different time points. Fig. 4*K* shows normal urine color before injection. At 30 min and 1.5 h postinjection, the urine becomes dark brown, which is characteristic of ZES-SPIONs elution. After 2.5 h postinjection,

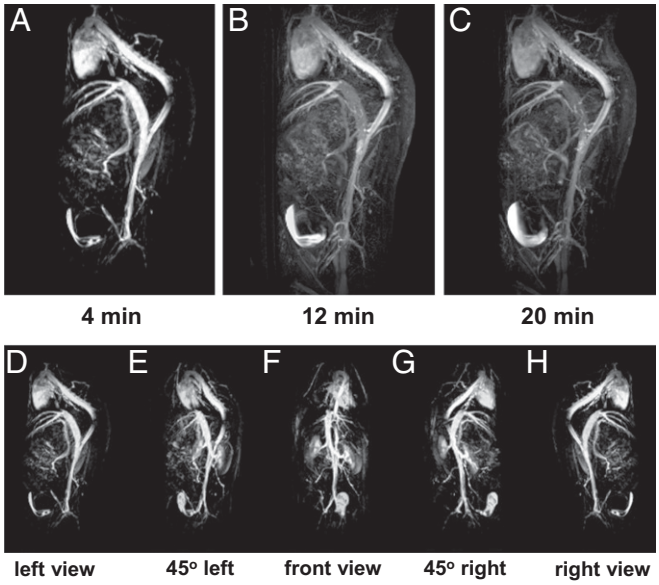

Fig. 5. (*A–C*) T_1-weighted magnetic resonance angiography (MRA) of a mouse injected with ZDS-coated exceedingly small SPIONs (ZES-SPIONs) at 7 T. The time points beneath each image are the time after injection of the ZES-SPIONs. (*D–H*) Five different perspectives of the MRA, which are extracted from the 3D scan, at the 4-min mark. A clear positive contrast of the heart and blood vessels are seen, and this positive contrast fades in time while the signal from the bladder increases, consistent with a renal excretion pathway.

the urine returns to its normal yellow color, indicating that the particle excretion happens mostly within the first 2.5 h, which is in agreement with the radioactive biodistribution data. Moreover, we performed relaxivity measurements on the ZES-SPIONs that were renally cleared (Table S2). The results show that the ZES-SPIONs in urine have an r_2/r_1 of 1.9, very close to the r_2/r_1 of ZES-SPIONs in PBS before injection. Together, these results indicate that ZES-SPIONs clear through the kidney efficiently as particles and their MR contrast power remains largely unchanged.

Next, we demonstrate the preclinical potential of our ZES-SPIONs as positive contrast agent for MR imaging (49, 50) in an animal model. We used a MRI scanner to image mice injected with ZES-SPIONs at a concentration of 0.2 mmol [Fe]/kg, comparable to the concentrations of GBCAs (~0.1–0.25 mmol [metal]/kg) administered in the clinic. The T_1-weighted MR images of one of the mice are shown in Fig. 4 and in Movies S1–S3. Fig. 4*A* shows a sagittal slice before the injection of ZES-SPIONs. Before injection the heart (red arrow), the vena cava (green arrow) and the bladder (yellow arrow) do not show appreciable positive contrast, as expected. Fig. 4*B* shows that the heart and the vena cava display strong positive contrast immediately after injection. Fig. 4*C* shows that, at 8 min after injection, the bladder displays some positive contrast, indicating an excretion of ZES-SPIONs. With the increase of time postinjection, Fig. 4 *D* and *E* show that the positive contrast in the bladder increases, suggesting an accumulation of ZES-SPIONs (see Movies S1–S3 and Fig. S4 for additional rat and mouse MRI data).

Fig. 4 *F–J* show a different sagittal slice at the same time points. Fig. 4*F* shows the absence of contrast before injection for the kidney (blue arrow). Immediately after injection, the kidney displays strong positive contrast enhancement. With increasing time postinjection, Fig. 4 *G–J* demonstrates continuing positive contrast enhancement in the kidney (Fig. S5*A*). These results suggest that our ZES-SPIONs can clear through the kidney at a rate that is consistent with the timescales used in multiphase dynamic imaging. Previously reported SPIONs have all have HDs that are larger than 5.5 nm, whereas the ZES-SPIONs here have a qualitatively smaller HD of 4.7 nm, which is smaller than the glomerular filtering threshold.

We further demonstrate the future preclinical potential of our ZES-SPIONs in T_1-weighted magnetic resonance angiography (MRA), an important clinical use of T_1-weighted contrast (51). Fig. 5 *A–C* shows MRA of a mouse injected with ZES-SPIONs at different time points. Due to the strong T_1 contrast and a circulation time that is sufficiently long, the blood vessels in this MRA study can be imaged with a spatial resolution of ~0.2 mm. Fig. 5 *A–C* shows strong positive contrast of the heart and blood vessels, which fades in time while the signal from the bladder increases, again consistent with a renal excretion pathway. The application of ZES-SPIONs as a blood pool agent can be further described by comparing signal-to-noise ratios (SNRs) in the vascular system and the less perfused tissues. Fig. 5 *D–H* shows different spatial perspectives of the MRA extracted from a three-dimensional (3D) scan (see Movies S4 and S5 for the full 3D scan). Here, contrast-to-noise ratio (CNR) between blood in the vena cava and muscle tissue increases from 4 (before injection) to 55 (after injection). The initial SNRs were 13 for blood and 9 for muscle, respectively; and after ZES-SPION administration, the SNRs were 65 and 10, respectively, showing a relative signal enhancement of fivefold in blood and essentially no pronounced signal enhancement in muscle. We note here also that the longer circulation times (the half-life in blood is ~19 min, which was measured by monitoring the T2* signal over time as shown in Fig. S5*B*) of ZES-SPIONs relative to the very rapid clearance of some Gd-based contrast agents such as Gd-DTPA (~2 min blood half-life) may provide an advantage in angiography. Moreover, the blood half-life of ZES-SPIONs is comparable to that of Gadofosveset [Ablavar; ~23 min (52)], a type of GBCA used for angiography. In addition, our future efforts will be geared toward the development of targeted formulations based on the presented ZES-SPIONs, such as by using thiol-maleimide conjugation strategies.

In summary, our results demonstrate that ZES-SPIONs have a small enough HD to show kidney clearance, and that their T_1 contrast power is high enough that these particles can be used for MRA and conventional positive MRI contrast. This is an example of a class of Gd-free MRI contrast agents that could be used for MRA in a way that is similar to the GBCAs. Furthermore, unlike existing SPION-based MRI contrast agents, which exhibit prolonged contrast and a potential for iron overload, the pharmacokinetic properties of ZES-SPIONs are such that long-term contrast changes may be avoided, and the iron dose that remains in the body can be kept in a safe range. This material system can be the basis for developing positive Gd-free MRI contrast agents as alternatives to GBCAs in the clinic.

Materials and Methods

Chemicals were obtained from Sigma-Aldrich and used as received unless specified. Air-sensitive materials were handled under dry nitrogen atmosphere with oxygen levels <0.2 ppm in an Omni-Lab VAC glove box. All solvents were purchased from EMD Biosciences and spectrophotometric grade. TEM images and energy-dispersive X-ray spectroscopy (EDX) of the SPIONs were obtained with a JEOL 200CX electron microscope operated at 120 kV and a JEOL 2010 electron microscope operated at 200 kV. ζ-Potential measurements were performed on a Malvern Instruments Nano-ZS90. Magnetization measurements were performed on a Quantum Design MPMS-XL SQUID. Mice for urine study were acquired from Charles River Laboratories International, and they were housed in the Division of Comparative Medicine at Massachusetts Institute of Technology in an Association for Assessment and Accreditation of Laboratory Animal Care-accredited facility. All mice were studied in accordance with approved institutional protocols at Massachusetts Institute of Technology and University Medical Center Hamburg–Eppendorf. Mice and rats were anesthetized by either i.p. injection of ketamine and xylazine or inhalation of isoflurane and oxygen gas. Additional experimental details about synthesis, characterizations, relaxivity measurements, and MR imaging are provided in *Supporting Information*.

ACKNOWLEDGMENTS. H.W. thanks Dr. Yong Zhang for his assistance with acquiring transmission electron microscopy images and Patrick Boisvert for his help with SQUID measurements. This work was supported by Massachusetts Institute of Technology (MIT)–Harvard NIH Center for Cancer Nanotechnology Excellence Grant 1U54-CA119349 (to M.G.B.), the Army Research Office through the Institute for Soldier Nanotechnologies (Grant W911NF-07-D-0004, to M.G.B.), the NIH-funded Laser Biomedical Research Center through Grant 9-P41-EB015871-26A1 (to M.G.B.), the MIT Deshpande Center Innovation Grant (to M.G.B.), NIH Grants R01-MH103160 and R01-DA028299 (to A.J.), and the European Union Seventh Framework Programme (FP7) Project RESOLVE (FP7-HEALTH-2012-305707) (to M.H.). O.T.B. was supported in part by a European Molecular Biology Organization long-term fellowship. D.M.M. was supported in part by a National Science Foundation graduate fellowship. S.O. was supported by a Japan Society for the Promotion of Science Postdoctoral Fellowship for Research Abroad.

1. Harisinghani MG, et al. (2003) Noninvasive detection of clinically occult lymph-node metastases in prostate cancer. *N Engl J Med* 348(25):2491–2499.
2. Centers for Medicare and Medicaid Services (2014) 2014 ASP Drug Pricing Files. Available at https://www.cms.gov/Medicare/Medicare-Fee-for-Service-Part-B-Drugs/McrPartBDrugAvgSalesPrice/2014ASPFiles.html. Accessed June 16, 2015.
3. Kim BH, et al. (2011) Large-scale synthesis of uniform and extremely small-sized iron oxide nanoparticles for high-resolution T1 magnetic resonance imaging contrast agents. *J Am Chem Soc* 133(32):12624–12631.
4. Lin CH, Cai SH, Feng JH (2012) Positive contrast imaging of SPIO nanoparticles. *J Nanomater* 2012:734842.
5. Seo WS, et al. (2006) FeCo/graphitic-shell nanocrystals as advanced magnetic-resonance-imaging and near-infrared agents. *Nat Mater* 5(12):971–976.
6. McDonald MA, Watkin KL (2006) Investigations into the physicochemical properties of dextran small particulate gadolinium oxide nanoparticles. *Acad Radiol* 13(4):421–427.
7. Bridot JL, et al. (2007) Hybrid gadolinium oxide nanoparticles: Multimodal contrast agents for in vivo imaging. *J Am Chem Soc* 129(16):5076–5084.
8. Hifumi H, Yamaoka S, Tanimoto A, Citterio D, Suzuki K (2006) Gadolinium-based hybrid nanoparticles as a positive MR contrast agent. *J Am Chem Soc* 128(47):15090–15091.
9. Na HB, et al. (2007) Development of a T1 contrast agent for magnetic resonance imaging using MnO nanoparticles. *Angew Chem Int Ed Engl* 46(28):5397–5401.
10. Caravan P, Ellison JJ, McMurry TJ, Lauffer RB (1999) Gadolinium(III) chelates as MRI contrast agents: Structure, dynamics, and applications. *Chem Rev* 99(9):2293–2352.
11. Todd DJ, Kagan A, Chibnik LB, Kay J (2007) Cutaneous changes of nephrogenic systemic fibrosis: Predictor of early mortality and association with gadolinium exposure. *Arthritis Rheum* 56(10):3433–3441.
12. Perez-Rodriguez J, Lai S, Ehst BD, Fine DM, Bluemke DA (2009) Nephrogenic systemic fibrosis: Incidence, associations, and effect of risk factor assessment—report of 33 cases. *Radiology* 250(2):371–377.
13. McDonald RJ, et al. (2015) Intracranial gadolinium deposition after contrast-enhanced MR imaging. *Radiology* 275(3):772–782.
14. Kanda T, et al. (2015) High signal intensity in dentate nucleus on unenhanced T1-weighted MR images: Association with linear versus macrocyclic gadolinium chelate administration. *Radiology* 275(3):803–809.
15. Kanal E, Tweedle MF (2015) Residual or retained gadolinium: Practical implications for radiologists and our patients. *Radiology* 275(3):630–634.
16. Errante Y, et al. (2014) Progressive increase of T1 signal intensity of the dentate nucleus on unenhanced magnetic resonance images is associated with cumulative doses of intravenously administered gadodiamide in patients with normal renal function, suggesting dechelation. *Invest Radiol* 49(10):685–690.
17. Frey NA, Peng S, Cheng K, Sun S (2009) Magnetic nanoparticles: Synthesis, functionalization, and applications in bioimaging and magnetic energy storage. *Chem Soc Rev* 38(9):2532–2542.
18. Park J, et al. (2005) One-nanometer-scale size-controlled synthesis of monodisperse magnetic iron oxide nanoparticles. *Angew Chem Int Ed Engl* 44(19):2873–2877.
19. Kim BH, et al. (2013) Sizing by weighing: Characterizing sizes of ultrasmall-sized iron oxide nanocrystals using MALDI-TOF mass spectrometry. *J Am Chem Soc* 135(7):2407–2410.
20. McCarthy JR, Weissleder R (2008) Multifunctional magnetic nanoparticles for targeted imaging and therapy. *Adv Drug Deliv Rev* 60(11):1241–1251.
21. Ittrich H, Peldschus K, Raabe N, Kaul M, Adam G (2013) Superparamagnetic iron oxide nanoparticles in biomedicine: Applications and developments in diagnostics and therapy. *RoFo Fortschr Geb Rontgenstr Nuklearmed* 185(12):1149–1166.
22. Weissleder R, et al. (1989) Superparamagnetic iron oxide: Pharmacokinetics and toxicity. *AJR Am J Roentgenol* 152(1):167–173.
23. Wang YXJ, Hussain SM, Krestin GP (2001) Superparamagnetic iron oxide contrast agents: Physicochemical characteristics and applications in MR imaging. *Eur Radiol* 11(11):2319–2331.
24. US Securities and Exchange Commission (2014) US Securities and Exchange Commission Filings, Item 8. Financial Statements and Supplementary Data. (AMAG Pharmaceuticals, Inc, Waltham, MA). Available at https://www.sec.gov/Archives/edgar/data/792977/000104746915000871/a2223053z10-k.htm. Accessed January 5, 2016.
25. Cunningham CH, et al. (2005) Positive contrast magnetic resonance imaging of cells labeled with magnetic nanoparticles. *Magn Reson Med* 53(5):999–1005.
26. Gossuin Y, Gillis P, Hocq A, Vuong QL, Roch A (2009) Magnetic resonance relaxation properties of superparamagnetic particles. *Wiley Interdiscip Rev Nanomed Nanobiotechnol* 1(3):299–310.
27. Hyeon T, Lee SS, Park J, Chung Y, Na HB (2001) Synthesis of highly crystalline and monodisperse maghemite nanocrystallites without a size-selection process. *J Am Chem Soc* 123(51):12798–12801.
28. Hao R, et al. (2010) Synthesis, functionalization, and biomedical applications of multifunctional magnetic nanoparticles. *Adv Mater* 22(25):2729–2742.
29. Park J, et al. (2004) Ultra-large-scale syntheses of monodisperse nanocrystals. *Nat Mater* 3(12):891–895.
30. Tromsdorf UI, Bruns OT, Salmen SC, Beisiegel U, Weller H (2009) A highly effective, nontoxic T1 MR contrast agent based on ultrasmall PEGylated iron oxide nanoparticles. *Nano Lett* 9(12):4434–4440.
31. Tromsdorf UI, et al. (2007) Size and surface effects on the MRI relaxivity of manganese ferrite nanoparticle contrast agents. *Nano Lett* 7(8):2422–2427.
32. Choi HS, et al. (2007) Renal clearance of quantum dots. *Nat Biotechnol* 25(10):1165–1170.
33. Woo K, et al. (2004) Easy synthesis and magnetic properties of iron oxide nanoparticles. *Chem Mater* 16(14):2814–2818.
34. Schladt TD, Graf T, Tremel W (2009) Synthesis and characterization of monodisperse manganese oxide nanoparticles-evaluation of the nucleation and growth mechanism. *Chem Mater* 21(14):3183–3190.
35. Wei H, Bruns OT, Chen O, Bawendi MG (2013) Compact zwitterion-coated iron oxide nanoparticles for in vitro and in vivo imaging. *Integr Biol* 5(1):108–114.
36. Clavijo Jordan MV, Beeman SC, Baldelomar EJ, Bennett KM (2014) Disruptive chemical doping in a ferritin-based iron oxide nanoparticle to decrease r2 and enhance detection with T1-weighted MRI. *Contrast Media Mol Imaging* 9(5):323–332.
37. Wei H, et al. (2012) Compact zwitterion-coated iron oxide nanoparticles for biological applications. *Nano Lett* 12(1):22–25.
38. Satat G, et al. (2015) Locating and classifying fluorescent tags behind turbid layers using time-resolved inversion. *Nat Commun* 6:6796.
39. Chen O, et al. (2014) Magneto-fluorescent core-shell supernanoparticles. *Nat Commun* 5:5093.
40. Strijkers GJ, Mulder WJ, Kluza E, Nicolay K (2006) The optimization of liposomal formulations for molecular MR imaging. *Proceedings of the International Society for Magnetic Resonance in Medicine* (The International Society for Magnetic Resonance in Medicine, Concord, CA), Vol 14, p 1835.
41. Lee H, Shin TH, Cheon J, Weissleder R (2015) Recent developments in magnetic diagnostic systems. *Chem Rev* 115(19):10690–10724.
42. Khurana A, et al. (2013) Ferumoxytol: A new, clinically applicable label for stem-cell tracking in arthritic joints with MRI. *Nanomedicine (Lond)* 8(12):1969–1983.
43. Weinstein JS, et al. (2010) Superparamagnetic iron oxide nanoparticles: Diagnostic magnetic resonance imaging and potential therapeutic applications in neurooncology and central nervous system inflammatory pathologies, a review. *J Cereb Blood Flow Metab* 30(1):15–35.
44. Schnorr J, et al. (2012) Cardiac magnetic resonance angiography using blood-pool contrast agents: Comparison of citrate-coated very small superparamagnetic iron oxide particles with gadofosveset trisodium in pigs. *Rofo* 184(2):105–112.
45. Kalavagunta C, Metzger GJ (2010) A field comparison of r1 and r2* relaxivities of Gd-DTPA in aqueous solution and whole blood: 3T versus 7T. *Proceedings of The International Society for Magnetic Resonance in Medicine* (The International Society for Magnetic Resonance in Medicine, Concord, CA), Vol 18, p 4990.
46. Bennett CL, et al. (2012) Gadolinium-induced nephrogenic systemic fibrosis: The rise and fall of an iatrogenic disease. *Clin Kidney J* 5(1):82–88.
47. Gaglia JL, et al. (2015) Noninvasive mapping of pancreatic inflammation in recent-onset type-1 diabetes patients. *Proc Natl Acad Sci USA* 112(7):2139–2144.
48. Freund B, et al. (2012) A simple and widely applicable method to ^{59}Fe-radiolabel monodisperse superparamagnetic iron oxide nanoparticles for in vivo quantification studies. *ACS Nano* 6(8):7318–7325.
49. Turetschek K, et al. (2001) Tumor microvascular characterization using ultrasmall superparamagnetic iron oxide particles (USPIO) in an experimental breast cancer model. *J Magn Reson Imaging* 13(6):882–888.
50. Huzjan R, Sala E, Hricak H (2005) Magnetic resonance imaging and magnetic resonance spectroscopic imaging of prostate cancer. *Nat Clin Pract Urol* 2(9):434–442.
51. Goyen M (2008) Gadofosveset-enhanced magnetic resonance angiography. *Vasc Health Risk Manag* 4(1):1–9.
52. Parmelee DJ, Walovitch RC, Ouellet HS, Lauffer RB (1997) Preclinical evaluation of the pharmacokinetics, biodistribution, and elimination of MS-325, a blood pool agent for magnetic resonance imaging. *Invest Radiol* 32(12):741–747.